Records of an ancient Martian magnetic field in ALH84001

Benjamin P. Weiss [a,*], Hojatollah Vali [b], Franz J. Baudenbacher [c],
Joseph L. Kirschvink [a], Sarah T. Stewart [a], David L. Shuster [a]

[a] *Division of Geological and Planetary Sciences, 170-25, California Institute of Technology, Pasadena, CA 91125, USA*
[b] *Electron Microscopy Centre, Department of Anatomy and Cell Biology and Department of Earth and Planetary Sciences,
McGill University, 3640 University Street, Montreal, QC Canada H3A 2B2*
[c] *Department of Physics and Astronomy, Vanderbilt University, 6301 Stevenson Center, Nashville, TN 37235, USA*

Abstract

Although Mars does not presently appear to have a global dynamo magnetic field, strong crustal fields have recently been detected by the Mars Global Surveyor above surfaces formed ∼3 or more Ga. We present magnetic and textural studies of Martian meteorite ALH84001 demonstrating that 4 Ga carbonates containing magnetite and pyrrhotite carry a stable natural remanent magnetization. Because $^{40}Ar/^{39}Ar$ thermochronology demonstrates that most ALH84001 carbonates have probably been well below the Curie point of magnetite since near the time of their formation [Weiss et al., Earth Planet. Sci. Lett. (2002) this issue], their magnetization originated at 3.9–4.1 Ga on Mars. This magnetization is at least 500 million years (Myr) older than that known in any other planetary rock, and its strong intensity suggests that Mars had generated a geodynamo and global magnetic field within 450–650 Myr of its formation. The intensity of this field was roughly within an order of magnitude of that at the surface of the present-day Earth, sufficient for magnetotaxis by the bacteria whose magnetofossils have been reported in ALH84001 and possibly for the production of the strong crustal anomalies. Chromite in ALH84001 may retain even older records of Martian magnetic fields, possibly extending back to near the time of planetary formation. © 2002 Elsevier Science B.V. All rights reserved.

Keywords: Mars; paleomagnetism; dynamos; magnetic methods; Martian meteorites; atmosphere; ALH84001

* Corresponding author. Tel.: +1-626-395-6187;
Fax: +1-626-568-0935.

E-mail addresses: bweiss@gps.caltech.edu (B.P. Weiss),
vali@eps.mcgill.ca (H. Vali),
franz.j.baudenbacher@vanderbilt.edu (F.J. Baudenbacher),
kirschvink@caltech.edu (J.L. Kirschvink),
sstewart@gps.caltech.edu (S.T. Stewart), dshuster@caltech.edu
(D.L. Shuster).

1. Introduction

The age of the crustal magnetization on Mars has been interpreted to be either older [2] or substantially younger [3] than several large, ∼3.0–4.2 Ga impact basins. At least 11 Martian meteorites have remanent magnetizations [4–10] that originated sometime after the rocks formed at 1300–180 Ma. Another Martian meteorite, ALH84001,

is an orthopyroxene cumulate which crystallized at 4.5 Ga [11] and contains ∼1% zoned carbonate. These carbonates contain magnetite and iron-sulfide [20] and have Rb/Sr and Pb/Pb ages of 3.90 ± 0.04 Ga and 4.04 ± 0.1 Ga, respectively [12] (although the Rb/Sr data have recently been questioned [13]). ALH84001 also possesses a stable magnetization that predates its ejection from Mars 15 million years ago (Ma) [4,14,15]. Because it is the oldest known Martian rock, ALH84001 may contain unique records of the earliest period of Martian magnetism and evolution [16].

Kirschvink et al. [14] argued that iron sulfide within the orthopyroxene of ALH84001 carries a stable magnetization, but were unable to demonstrate that the meteorite's carbonates are magnetized. Based on a paleomagnetic conglomerate test on two adjacent ALH84001 orthopyroxenite grains, they suggested that the meteorite has been cooler than 110°C since before the formation of the fracture surface separating the grains. They assumed this fracture was part of the internal crushed zone created during the 'D1' shock event [17]. However, subsequent studies (see Section 5) have identified flow textures and vesicles in feldspathic glass that intrudes and disrupts carbonates, suggesting that one or more high-temperature shock events (with peak pressures of >45 GPa and temperatures >1400°C) affected at least part of the meteorite after the D1 event [17–19]. Because no carbonates were identified on the fracture surface separating Kirschvink et al.'s two grains, this fracture need not have formed during D1 but instead could date to any time between 4.0 Ga and 15 Ma. Thus, their thermal constraint may not apply to before the time of carbonate formation, but instead extend back to a more recent but unknown time. More detailed magnetic studies by Weiss et al. [15] have shown that the transfer of ALH84001 from Mars to their laboratory, including the impact at 15 Ma that ejected it from the Martian surface and its passage through the Earth's atmosphere, did not heat the interior of the meteorite above ∼40°C for even short periods of time (<10 min). It is unknown how much further back in time beyond 15 Ma this 40°C thermal constraint applies.

2. Samples and methods

We analyzed two unoriented and two oriented subsamples of ALH84001 for this study. ALH-84001,232e (Figs. 1–3) is a 1 mm thick slice from the interior of the meteorite previously studied by Weiss et al. [15]. Slice 232e was cut from subsample ALH84001,232 with a diamond-impregnated wire saw and mounted on a glass slide with cyanoacrylic cement [15]. An unoriented subsample of ALH84001,236 was used for high resolution transmission electron microscopy (TEM) imaging (Fig. 4). TEM data on 594 individual ALH84001 magnetite crystals used for our blocking temperature calculations (Fig. 5) were measured by Thomas-Keprta et al. after extraction from another unoriented subsample [20]. Our anhysteretic remanent acquisition studies (Fig. 6) were conducted on a second unoriented pyroxenite grain from ALH84001,236 weighing ∼20 mg and containing zoned carbonate. Finally, subsample 227b (Figs. 7–9) is an oriented 30 μm thin section taken from near the meteorite's fusion crust. The thin section was set with cyanoacrylic cement at room temperature so that its natural remanent magnetization (NRM) was preserved. ALH84001,232e and 227b were also both analyzed with backscatter scanning electron microscopy (SEM) (Figs. 1, 2 and 8).

Field emission gun transmission electron microscopy (FEG-TEM) data were taken from an ultrathin section prepared from a zoned carbonate in 232e (identified in [15]), taken from just below the tip of the bottommost arrow in Fig. 1a using a micro sampling device on a Hitachi FB-2000A focus ion beam system (Fig. 2). This system allows non-destructive preparation of an ultrathin section in situ with a precision of 1 μm without exposing the sample to water, epoxy resin, or other contaminants. The bright field (Fig. 3a,e), compositional (Fig. 3b–d), and selected area electron diffraction (Fig. 3e, inset) data were acquired on this section with a Hitachi HF 2200 cold field emission analytical TEM, using an acceleration voltage of 200 kV and a camera length of 80 cm. The patterns of single crystal and polycrystalline magnesite present in the section were used as an internal standard. The lattice plane spacings, *d*,
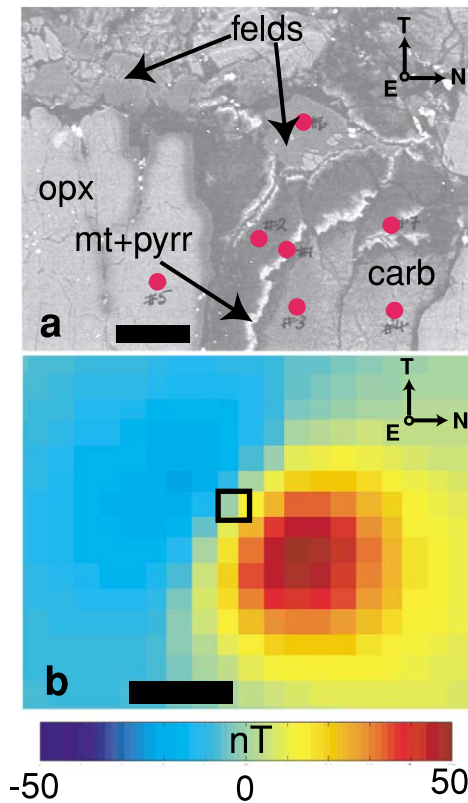
Fig. 1. Compositional and magnetic maps of a portion of 1 mm thick slice ALH84001,232e, centered on the carbonate found 100 μm below the surface by Weiss et al. [15]. (a) Backscattered SEM image showing orthopyroxene, zoned carbonate (with dark Mg-carbonate rim bounded by two bright bands of magnetite and pyrrhotite), feldspathic glass, and fractures (dark black lines). The compositions of these phases were confirmed by X-ray spot analyses taken at the locations marked by red circles. A cross-section of the carbonate was later extracted for FEG-TEM analyses (Fig. 3) from the boundary between the Mg-carbonate and inner band of magnetite and pyrrhotite, just below the tip of the bottom arrow (Fig. 2). (b) Ultrahigh resolution scanning SQUID Microscope (UHRSSM) image centered on same location as a, showing the intensity of the eastward (out-of-the-page) component of the magnetic field as observed ∼200 μm above the sample. The sample had been heated to 360°C in a zero field (<10 nT) prior to UHRSSM imaging. The SEM image in a was taken from roughly the location marked by the black box at the center. North is to the right and Top is toward the top of the page, as demonstrated by the compass registered to the Johnson Space Center curatorial orientation system. Red (blue) regions correspond to eastwardly (westwardly) oriented fields. Scale bars are 20 μm (a) and 500 μm (b), and the color bar is in nT.

were calculated using the formula $d = \lambda L/r$, where λ is the wavelength of the electron beam at 200 kV, L is the camera length and r is the distance of a given pattern to the center of the primary beam (see Table 1). As the center of the primary beam cannot be accurately determined, the value of r is measured from the distance between two radially symmetrical patterns divided by 2. The diffraction pattern was taken from a selected area on a low magnification image (10 000×).

To conduct the anhysteretic remanent magnetism (ARM) acquisition test, we demagnetized the samples using a sinusoidally oscillating alternating field (AF) whose amplitude decayed from 100 mT to zero. We then gave the sample an ARM by subjecting it to a 0.2 mT DC bias field superimposed on the same AF. The intensity of magnet-
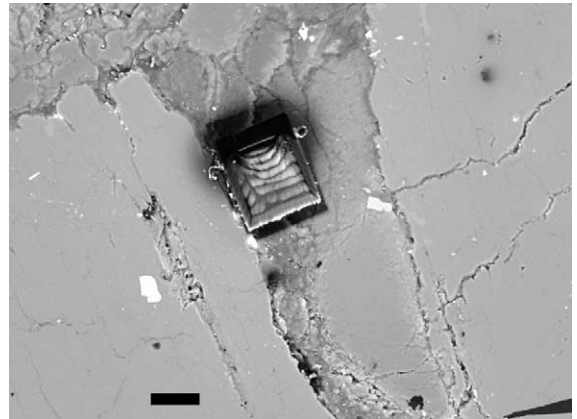

Fig. 2. Backscattered SEM image of carbonate from ALH-84001,232e (at location just below bottommost arrow in Fig. 1a) after an ultrathin section was prepared for FEG-TEM analysis (Fig. 3). A micro sampling device on a Hitachi FB-2000A focus ion beam (FIB) system progressively milled into the sample, producing an ultrathin section 20 μm wide by 20 μm long by 80 nm thick. The ultrathin section was initially prepared by cutting a wedge of thickness 5 μm by combined step and trench milling. The wedge was transferred and mounted on a compatible FIB/TEM holder using a mechanical probe. To reach the desired thickness and location of the ultrathin section, the wedge was then gradually ion-milled by transferring the specimen back and forth between the FIB and the TEM. A scanning mode in both FIB and TEM was used to monitor this procedure. This system allows non-destructive preparation of an ultrathin section in situ with a precision of 1 μm without exposing the sample to water, epoxy resin or other contaminants. The scale bar is 20 μm.
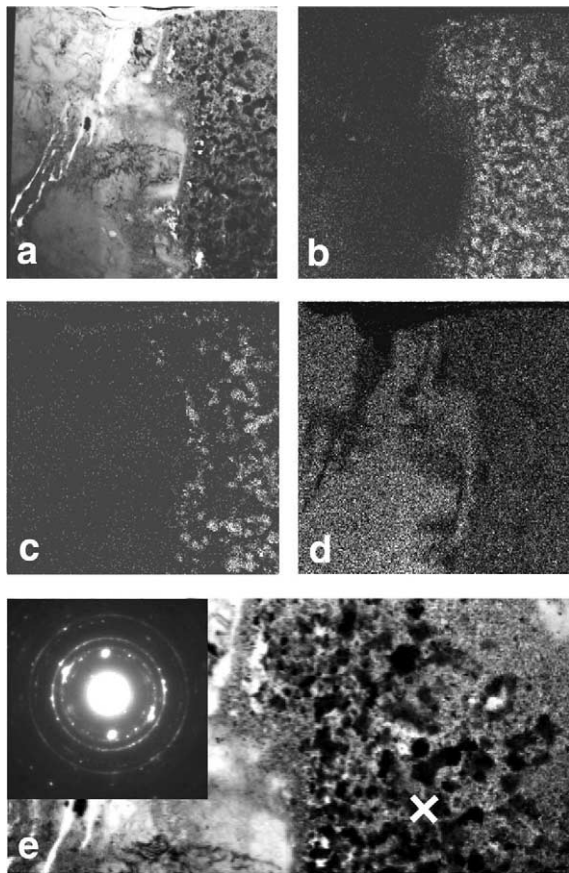
Fig. 3. Field emission gun transmission electron microscopy (FEG-TEM) data from the fine-grained particles present within the rim of the carbonate from ALH84001,232e identified by Weiss et al. [15]. As depicted in Fig. 2, a vertical slice of thickness ∼80 nm was prepared perpendicular to the image plane in Fig. 1. (a) High resolution bright field image showing individual magnetite and pyrrhotite crystals embedded in Mg–Ca–Fe-carbonate (right) adjacent to Mg-carbonate rim (left). (b–d) High resolution (1 nm) X-ray compositional maps of same region as a showing abundance of Fe (b), S (c), and Mg (d). A comparison of b and c with our O maps taken from the same location (not shown) demonstrates that many individual crystals simultaneously contain either Fe and S or Fe and O, demonstrating the presence of iron sulfides and iron oxides. (e) Higher magnification bright field image taken from top of a, with superimposed selected area electron diffraction pattern measured at the location marked by x. The lattice plane spacings corresponding to the pattern are diagnostic of pyrrhotite (4.73, 2.61, and 2.06 Å), magnetite (4.84 and 2.53 Å), and Mg-carbonate (2.75 and 2.11 Å). For a complete list of observed lattice plane spacings, intensities and their corresponding Miller indices, see Table 1. Each frame in a–d has a width of 7 μm, and frame e has a width of 5 μm.

ization of the sample was measured, and then the grain was given a new ARM with a larger DC bias field and its magnetization remeasured (Fig. 5). This process was repeated until reaching a bias field of 2 mT. Control ARM acquisition tests were measured using the same protocol on MV-1 magnetotactic bacteria and chiton teeth. All of the above magnetic measurements were made with a 2G™ Superconducting Rock Magnetometer in a class 1000 magnetically shielded (<100 nT) clean laboratory at Caltech.

Images of sample magnetic fields were obtained with the ultra high resolution scanning SQUID microscope (UHRSSM) [21,22], a DC-SQUID magnetometer with a DC-field sensitivity of ∼75 pT that maps the perpendicular component of the magnetic field of samples with better than 250 μm spatial resolution. SQUID microscopes with somewhat lower sensitivity and spatial resolution have been used in a variety of previous paleomagnetic studies [15,23–26]. The UHRSSM measurements were made in a magnetically shielded environment at Vanderbilt University (ambient field <10 nT).

3. The magnetized minerals in ALH84001

To determine the mineralogy of the magnetic phases in ALH84001, we conducted SEM (Figs. 1a and 2) and FEG-TEM analyses (Figs. 2 and 3 and Table 1) of the Fe-rich rim of a carbonate in ALH84001,232e. These data demonstrate the presence of magnetite (Fe_3O_4) and pyrrhotite ($Fe_{1-x}S$ for $x < 0.13$) in the carbonate rims. FEG-TEM compositional maps of Fe, S, Mg (Fig. 3a–d), O, Mn, K, Al and Ca (not shown) taken from the same location resolve individual crystals of pyrrhotite and magnetite in the single domain (SD) to superparamagnetic (SP) size range. Our SEM and FEG-TEM imaging (Figs. 1a and 2) show that a typical zoned carbonate is composed of ∼1 wt% pyrrhotite and magnetite in a mass ratio of ∼0.3–0.5. This mineralogy is also indicated by our high resolution TEM data from another carbonate in ALH84001,236 (Fig. 4). Our rock magnetic analyses on three ∼15 mg ALH84001 pyroxenite grains containing carbon-
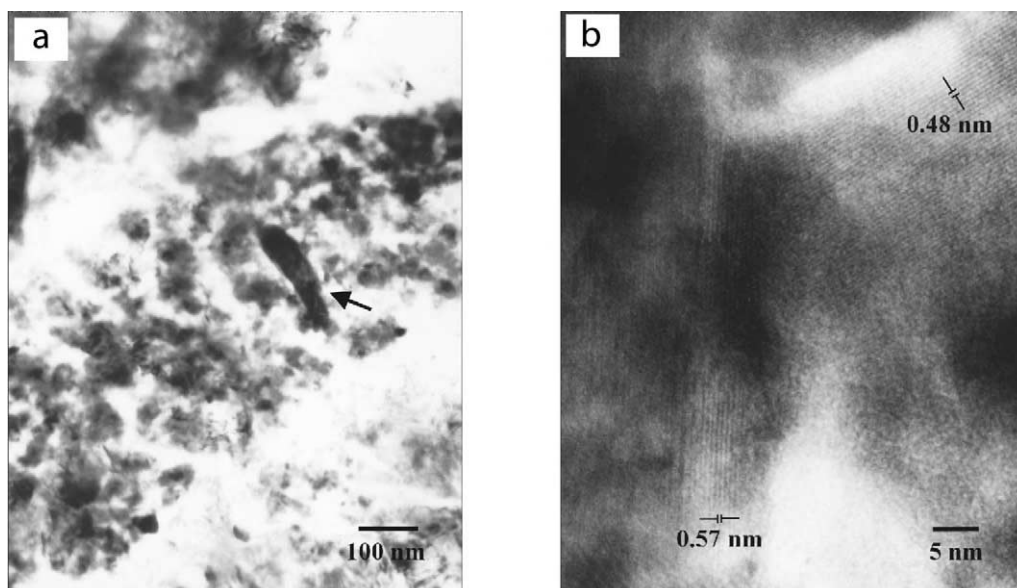
Fig. 4. High resolution TEM images of the Fe-rich rim of a zoned carbonate from ALH84001. (a) Low magnification image showing iron sulfide (arrow) and iron oxide. (b) High resolution image of the edge of the sulfide and an adjacent oxide showing the lattice fringes of 0.48 nm and 0.57 nm, diagnostic of pyrrhotite ($Fe_{1-x}S$ for $x < 0.13$) and magnetite (Fe_3O_4), respectively. Greigite, whose lattice also has a 0.48 nm spacing, is unstable under the electron beam and so cannot explain these data (e.g., Taylor, A.P., Magnetotactic Bacteria and Their Biominerals, Ph.D. Thesis, The University of Queensland, 2001).

ates [14,15] again demonstrate that the meteorite contains magnetic crystals ranging from SP to PSD in size. Thomas-Keprta et al. [20] found that 594 individual magnetite crystals extracted from the carbonate are nearly stoichiometric (Ti, Al, and Cr < 0.1%) and in the SD (∼70% of grains) to SP (∼30% of grains) size range. Low temperature cycling [15] indicates that ALH84001 magnetites have a composition $Fe_{3-x} Ti_xO_4$ with $x < 0.01$. Magnetite of this composition has a Curie point of close to 580°C [27]. Thermal demagnetization of ALH84001,232e [15] demonstrates that the meteorite has blocking temperatures from less than −263°C to well in excess of 200°C. Our data presented below (Fig. 1b) further extend this range by demonstrating that the meteorite remains strongly magnetized after zero-field heating to > 360°C. A comparison of the size and shape distribution measured by Thomas-Keprta et al. [20] with our Néel theory calculations of the temperature dependence of the SP–SD boundary confirms that the ALH84001 magnetites have blocking temperatures up to 580°C (Fig. 5). These observations demonstrate that, despite sugges-

tions to the contrary [9], stoichiometric magnetite should dominate the remanent magnetism of carbonates in ALH84001 (with pyrrhotite only significantly contributing to the low blocking temperature fraction).

The tight packing of the magnetite and pyrrhotite in the carbonates (Fig. 3) suggests that these crystals should be magnetostatically interacting. We examined this possibility using an ARM acquisition test on a subsample of ALH84001,236 (see Section 2). The linearity and shallow slope of the meteorite's ARM acquisition curve (Fig. 6) gives strong evidence of magnetostatic interactions. Additional evidence for these interactions comes from the fact that both this grain and ALH84001,190 (the latter studied by Kirschvink et al. [14]) have isothermal remanent magnetism (IRM) acquisition and AF demagnetization of IRM curves that intersect at about 35% of the saturation IRM. The presence of these interactions indicates that it might be difficult to use standard techniques [28,29] to precisely measure the paleointensity of the field that magnetized ALH84001.
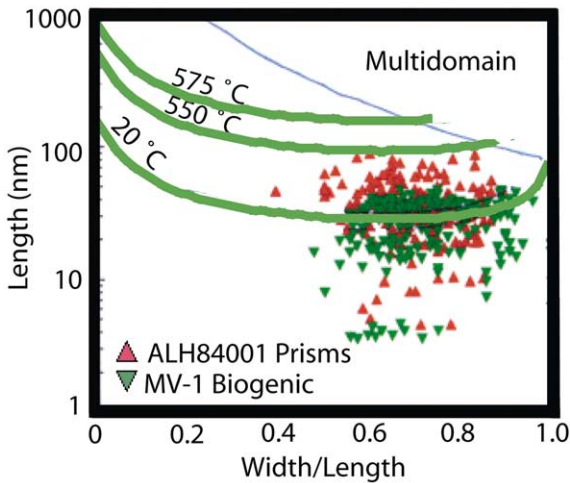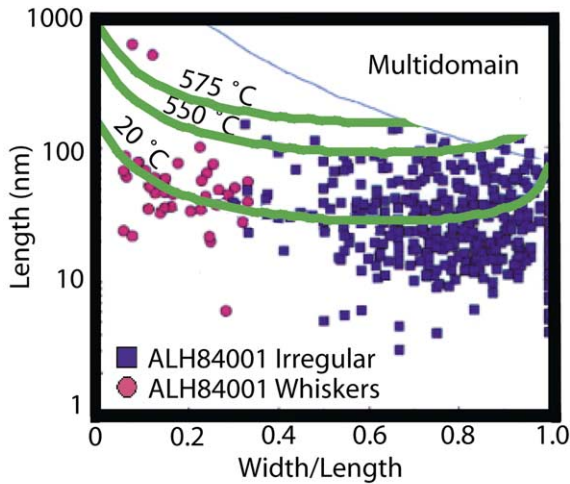
Fig. 5. The blocking temperature of magnetite calculated as a function of crystal size and shape and compared to the natural size distribution of inorganic (top) and fossil-like (bottom) magnetite in ALH84001 carbonate. Each green curve represents the SD–SP boundary for various temperatures as a function of crystal length and crystal length-to-width ratio. We assume a parallelepiped grain shape (as has been observed for ALH84001 magnetite [20]) and an unblocking time of 100 s. We calculated these curves following the methods of Butler and Banerjee [65] as modified by Diaz Ricci and Kirschvink [66]. The blue curve in each diagram represents the single domain–multidomain boundary. The curves have been overlaid onto the actual distribution of magnetite in ALH84001 carbonate, as measured by Thomas-Keprta et al. [20]. The diagrams demonstrate that ALH84001 carbonates contain magnetite with blocking temperatures up to its Curie point of 580°C.
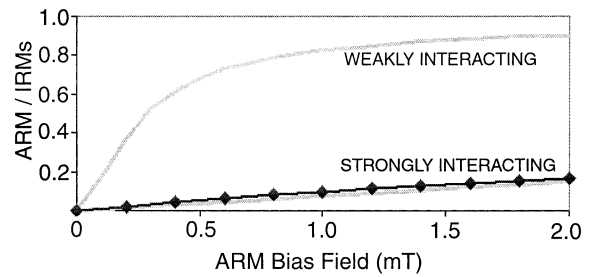

Fig. 6. Anhysteretic remanent magnetism (ARM) acquisition experiments on a ∼20 mg pyroxenite grain with zoned carbonate taken from ALH84001,236. The plot depicts the anhysteretic magnetic moment (normalized to the isothermal saturation magnetic moment) of three samples for a given DC bias field (see Section 2): ALH84001,236 (heavy black line), non-interacting MV-1 bacterial magnetosomes (top gray line), and highly interacting chiton tooth magnetite (bottom gray line).

4. SQUID microscopy

We have used the UHRSSM to map the vertical component of the remanent magnetic fields of ALH84001,227b,1 (Figs. 7 and 8) and a carbonate [15] from ALH84001,232e (Fig. 1). In order to examine the thermal stability of the magnetization in the meteorite, 232e was progressively thermally demagnetized at temperatures up to 360°C in a zero field (< 10 nT) prior to final imaging with the UHRSSM (Fig. 1b). A comparison of the UHRSSM data with the electron microscopy and X-ray spot analyses shows that nearly all of the magnetic fields above the interior of these samples are directly associated with zoned carbonate, identified in both 227b (Fig. 8c–f,h,k–m) and 232e (Figs. 1 and 3), and a few irregular unzoned carbonate patches, as identified in 227b (Fig. 8c,d). The latter carbonates are more calcic than the zoned carbonates and do not show a distinct, Fe-rich and Mg-rich rim (similar unzoned carbonates were recently identified by Eiler et al. [30] as the likely products of shock-melting of zoned carbonate). Several chromite grains also exhibit a weak magnetization (Fig. 8a,b,e,f,j). The 1 mm thick fusion crust on the exterior of the meteorite (Fig. 8b,d,g) was produced during passage through the Earth's atmosphere during which it was strongly magnetized by the Earth's field (Fig. 8a,c). As has been previously observed

[15], this remagnetized zone extends no further than ∼1 mm into the interior of the meteorite. A comparison of UHRSSM images of the carbonate in 232e taken before heating [15] and after thermal demagnetization at temperatures of 360°C (Fig. 1b) confirms our expectation that the carbonate has magnetic blocking temperatures from room temperature to well beyond 360°C. Other than the magnetite, pyrrhotite, fusion crust, and chromite, we did not identify any other ferromagnetic grains in the 227b thin section; no other magnetic features in the UHRSSM map can be associated with other minerals, and no other ferromagnetic minerals have ever been found in the meteorite.

Most of the magnetization associated with the carbonates is stable and remanent. Langevin theory [27] demonstrates that a typical ALH-84001 carbonate (with a radius of ∼50 μm and containing ∼10^8 SP and SD grains of magnetite and pyrrhotite) immersed in a 10 nT laboratory field will produce an induced magnetic field of <0.1 nT at the height of the UHRSSM pickup coil. Because the UHRSSM measures fields of ∼100 nT above single carbonates like that in

Figs. 1b and 8e, their magnetization cannot be induced but must be a remanence. Furthermore, magnetite's Pullaiah diagram [27] suggests that ALH84001 magnetites with 10 min blocking temperatures ∼>150°C would not acquire viscous remanence during residence on the Martian surface (assuming <−50°C for 4 Gyr), transfer through space to Earth (assuming <0°C for 15 Myr), and residence in Antarctica (assuming <0°C for 11 kyr) and America (<20°C for 17 yr).

To confirm that the carbonates, chromite, and fusion crust are actually the source of the magnetic field observed with the UHRSSM, we performed inversions to obtain the magnetization distribution that best reproduces (in a least squares sense) the fields above 227b. Although there is in general no unique magnetization distribution that can be associated with measurements of a given magnetic field pattern outside a magnetized region, such an inversion can be made solvable by assuming that the sample's magnetization is in the form of a grid of N evenly spaced dipoles confined to a plane within the sample. This two-dimensional 'equivalent source' method

Table 1
Mineralogy identified by selected area electron diffraction analysis (SAED) on an ultrathin section of ALH84001 carbonate

SAED *d*-spacing (Å)	Mineral name	Reference *d*-spacing (Å)	Miller indices (*hkl*)
4.84	Magnetite	4.852	(111)
4.73	Pyrrhotite	4.7	(113)
2.75	Magnesite	2.742	(104)
2.61	Pyrrhotite	2.633	(224) (404)
2.53	Magnetite	2.532	(311)
2.42	Magnetite	2.424	(222)
2.11	Magnesite	2.102	(113)
2.06	Pyrrhotite	2.054	(228)
1.96	Magnesite	1.939	(022)
1.71	Magnesite	1.7	(116) (018)
1.61	Magnetite	1.616	(511)
1.36	Magnesite	1.354	(119)
1.26	Magnetite	1.266	(622)
1.06	Magnesite	1.051	(226)
0.88	Magnetite	0.88	(931)
0.80	Magnetite	0.808	(1022)

Shown is a list of the *d*-spacings (first column) and their corresponding mineral name (second column) for the diffraction patterns observed in the SAED image (Fig. 3e, inset) obtained from the ultrathin section prepared from the Fe-rich area in ALH84001,232e (Fig. 2). The X-ray reference *d*-spacings obtained from the powder diffraction file database and their associated Miller indices (*hkl*) are listed in the third and fourth columns, respectively.
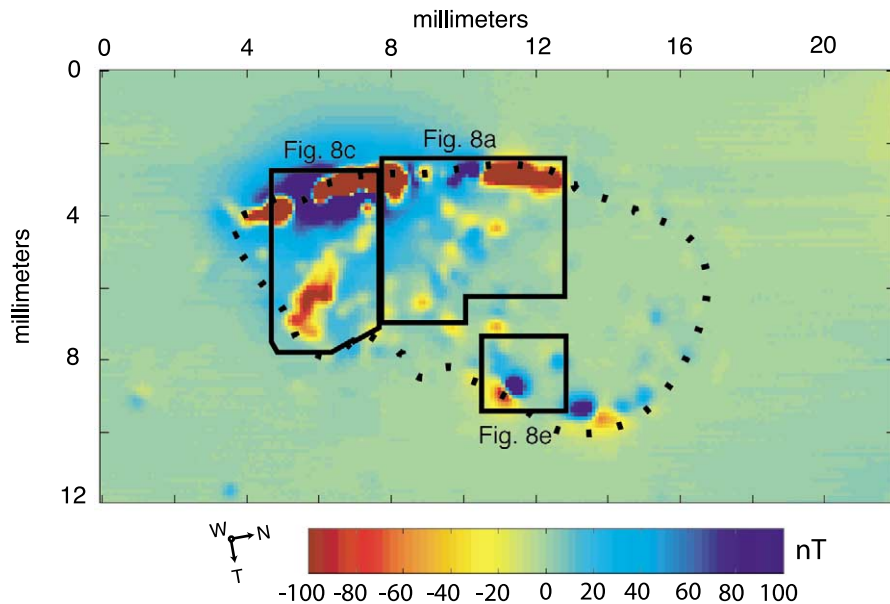
Fig. 7. The complete UHRSSM scan of ALH84001,227b,1 showing westward (out-of-the-page) component of the magnetic field ~ 130 μm above the sample. The boxed regions correspond to the various parts of 227b imaged in Fig. 8. The border of the thin section has been outlined with a dotted line on the UHRSSM scan. The compass is registered to the Johnson Space Center curatorial orientation system.

provides a good approximation for retrieving the magnetization of the 30 μm thin section 227b, whose magnetic field was measured at a height ~ 4 times its thickness. The method, commonly employed to invert aeromagnetic and satellite magnetic field data sets for crustal magnetizations (e.g., [31]), involves determining the size of the three vector components of the moment of each of the dipoles in the grid. The positions of the N dipoles were fixed while their individual moments and directions were allowed to vary, so that $3N$ parameters were solved for. Our inversions were implemented in MATLAB on a Sun Ultra 10 workstation. The UHRSSM data taken over several different regions of 227b were taken as subsets and an inversion was performed individually on each subset. An example of one such inversion is presented in Fig. 9. For each of the data subsets, we performed the equivalent source scheme twice, once using conjugate gradient analysis (a sparse matrix method which takes advantage of the rapid decay of dipole magnetic fields with distance) [32], and then again using singular value decomposition [33]. Both approaches solve for

the smallest possible normed magnetization consistent with the field data, and both yielded similar magnetization solutions.

The inversions (e.g., Fig. 9) confirm that carbonates, chromite, and fusion crust are the source of magnetic fields observed above our samples. The inversions (Fig. 9) also demonstrate that regions of the 227b thin section rich in carbonate-bearing magnetite and pyrrhotite (e.g., Fig. 8h,m) have magnetizations of ~ 0.1–1.6 A/m. Given the fractional abundance of carbonate in these regions, this would suggest that the carbonates have magnetizations of a few A/m.

A small patch of carbonate in 227b has been disaggregated and transported by melted feldspathic glass (Fig. 8f,l,m), during which its magnetization direction (Fig. 8e) appears to have rotated with respect to that of carbonates elsewhere in the thin section (Fig. 8c). This change in direction probably resulted from thermal remagnetization of the carbonate due to heating within the hot glass, although it may have also been partly the result of physical rotation of the carbonate. A less likely possibility is that the carbonates formed
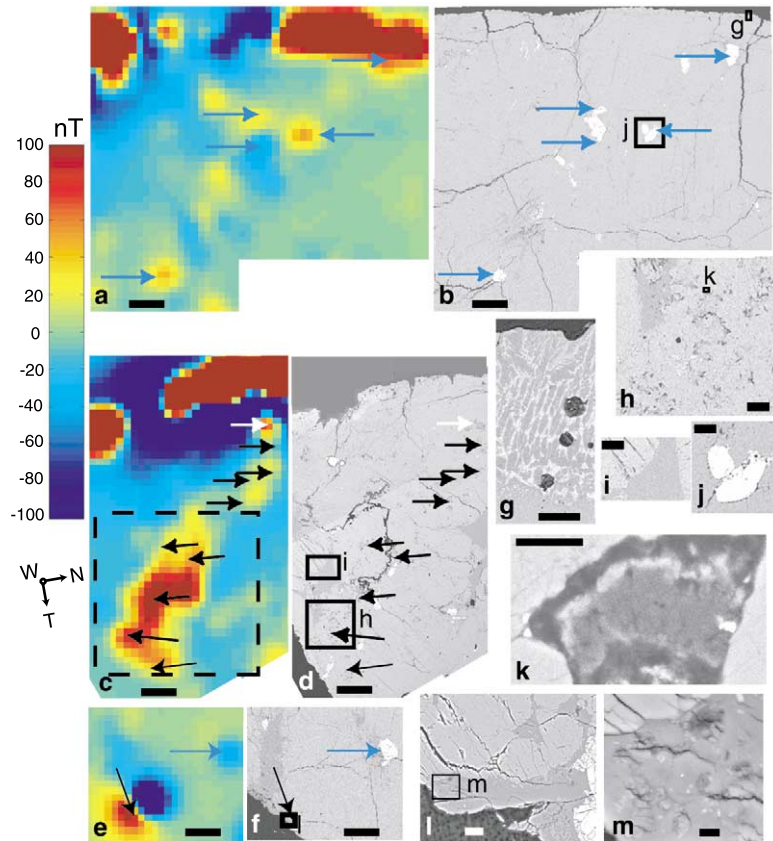
Fig. 8. Magnetic and compositional maps of selected portions of 30 μm thin section ALH84001,227b,1. For the complete magnetic map, see Fig. 7. (a) UHRSSM image showing westward (out-of-the-page) component of the magnetic field ~130 μm above the sample. The compass is registered to the Johnson Space Center curatorial orientation system. (b) Backscattered SEM image of same field as (a) showing orthopyroxene (light gray), feldspathic glass (dark gray), chromite (white grains, including those marked by blue arrows), and fusion crust discontinuously lining the top of the sample. The ~0.1 mm thick fusion crust was strongly magnetized during the meteorite's passage through the Earth's atmosphere. (c,d) UHRSSM and SEM images of a different portion of the same thin section with zoned carbonate containing magnetite and pyrrhotite (black arrows) and unzoned carbonate (white arrow). Strongly magnetized fusion crust lines the top of the sample, with a notch in the middle. A least squares magnetization inversion for the UHRSSM data enclosed by dashed box in c is presented in Fig. 9. (e,f) UHRSSM and SEM images of a different portion of the same thin section with magnetized chromite (blue arrow) and zoned carbonate (black arrow) containing magnetite and pyrrhotite. (g–m) Higher magnification SEM images of selected portions of b, d, and f: fusion crust (g); two lightly fractured, subhedral magnetized chromites (j); unfractured feldspathic glass surrounded by fractured orthopyroxene (i) that is adjacent to a patch of magnetized carbonate in a granular band of orthopyroxene (h,k); heavily fractured zoned carbonate that has been disaggregated and transported by feldspathic glass (l,m). Carbonate is dispersed throughout most of the glass visible in l. Magnetized chromites are labeled with blue arrows in a,b,e,f. Scale bars are 500 μm (a–f), 100 μm (h–j), 20 μm (g,l), and 3 μm (k,m).

over a period of time during which the absolute orientation of the local magnetic field changed. It is clear from our magnetization inversions (e.g., Fig. 9) that carbonates, although locally magnetized in a single direction (as in the case of the patch of carbonate at the bottom of Fig. 8c), are as a whole magnetized in at least three different directions: compare orientations of dipoles associated with carbonates in Figs. 1b and 8c,e.

Chromite grains are volumetrically more abundant than carbonate in 227b by at least an order of magnitude, but only in some cases have a de-

tectable magnetic signature (Fig. 8a,b,e,f,j). Although stoichiometric chromite ($FeCr_2O_4$) is paramagnetic at room temperature, Mg- and Al-rich chromites similar to those in ALH84001 (which have a mean composition of roughly $Fe_{1.05}Cr_{1.31}Al_{0.35}Mg_{0.20}Ti_{0.06}O_{4.0}$) [34] have been found to have Curie points above 300°C [35,36]. Furthermore, no exsolution lamellae have ever been identified in the ALH84001 chromites (despite searches for them [37]), suggesting that the magnetization in the chromites may be intrinsic to these phases rather than originating from intimately exsolved magnetite. The anomalies associated with the chromites in ALH84001 are approximately dipolar, with orientations in at least two and possibly three different directions. There are at least three westwardly magnetized chromites in Fig. 8a and an eastwardly one in Fig. 8e, while the second and third labeled chromites from left in Fig. 8a could be unidirectionally magnetized in a third direction. Thus, much of the spatial heterogeneity of magnetization observed previously [4,14,15] is the signature of carbonate and chromite magnetized in multiple directions.

5. Thermal constraints on the carbonate

There is considerable debate about whether carbonates in ALH84001 were heated during or after their formation at 4 Ga [17,30,38–41]. This is critical because determining the age of the magnetization in the carbonates requires knowing the last time they were heated above the Curie point of magnetite (580°C at a pressure of 1 bar). Even brief ($\ll 1$ s) excursions above the Curie point would be sufficient to completely remagnetize the meteorite.

One of the most likely processes that heated the meteorite is shock resulting from impacts on the Martian surface. As discussed in Section 1, ALH84001 has clearly been affected by multiple shock events [17–19]. However, despite their high peak temperatures, these shocks did not necessarily remagnetize the meteorite. This is because the pressure dependence of magnetite's Curie point has never been measured for high pressure shocks. In fact, if the very steep rise of the Curie point
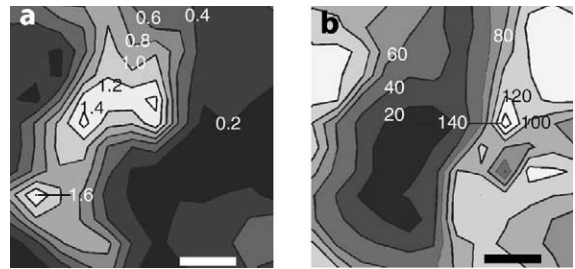

Fig. 9. Magnetization inversion of UHRSSM data from a selected portion of ALH84001,227b,1 (dashed boxed region of Fig. 8c), obtained with an equivalent source scheme solved by conjugate gradient analysis. A grid of $N = 144$ regularly spaced dipoles was used, and the total number of UHRSSM measurements in the boxed region was 576. (a) Contour plot of magnetization (A/m). (b) Contour plot of inclination of magnetization, where 0° is oriented directly upwards and 90° is in the plane of the thin section. Another equivalent source inversion solved by singular value decomposition gave nearly identical results. The contour lines in a are 0.2, 0.4, 0.6, 0.8, 1.0, 1.2, 1.4, and 1.6 A/m, with brighter regions having larger values. The contour lines in b are 20°, 40°, 60°, 80°, 100°, 120°, and 140°, with brighter regions having larger values. The scale bars are 500 μm. Because in these inversions we did not take into account the finite size of the UHRSSM's pickup coil (which has a diameter of 250 μm = 2.5 pixels), the actual size of the strongly magnetized region in the center-bottom of a should be a few pixels smaller in both the horizontal and vertical directions.

with pressure (20°C GPa^{-1}) that has been measured at hydrostatic pressures up to 0.6 GPa [42] continues to hold true at higher shock pressures, this would suggest that the peak temperatures produced during shocks might not completely remagnetize rocks. In that case, only shocks with post-shock temperatures exceeding the Curie point would be capable of remagnetizing rocks.

A second caveat is that it is probable that like most shocked rocks, ALH84001 has been heterogeneously deformed and heated by the shock events it has experienced (see Section 6). Given that at least one and possibly multiple shocks occurred after formation of the carbonates (see below), this means that some carbonates probably have been significantly heated one or more times while others may have experienced fewer or even no heating events. For the purposes of dating the magnetization in the carbonates, we will consider both possibilities: carbonates that may have been heated and those not heated since they formed.

Petrographic studies [17] have identified one major shock event that occurred after the formation of the carbonates. This is confirmed by our SEM and X-ray spot analysis data on the carbonate in slice 232e (Fig. 1a) and 227b (Fig. 8d,f,h,i,k), which demonstrate that like many ALH84001 carbonates, it is adjacent to anhedral feldspathic glass. This glass, which has been observed elsewhere in the meteorite [17–19] and lacks even short-range order [17,43], does not retain the shape of a relict feldspar crystal, is unfractured (unlike its immediate surroundings), fills irregular cracks and voids in the pyroxene, and even occasionally intrudes and disaggregates carbonate (see Fig. 8f,l,m and [18]). All of these observations indicate that the glass in our samples and throughout ALH84001 was melted and mobilized one or more times (the last such event was labeled 'D3' by Treiman [17]). Because microfaults in the 232e carbonate do not extend into the adjacent glass (Fig. 1a) and the glass occasionally intrudes 227b carbonate (Fig. 8l,m), it appears that at least some of the glass melted after the carbonates formed. Because the glass was hot enough to flow during this event, the intruded carbonate and any nearby material probably experienced a shock with peak pressures of 40–60 GPa [17,44] and post-shock temperatures of 400–1000°C [44,45]. These post-shock temperatures should have remagnetized most of the magnetite and pyrrhotite adjacent to the melted glass.

On the other hand, several geochemical studies of oxygen isotope and cation gradients in ALH-84001 indicate that other, unfractured carbonates have not been significantly heated since they formed at 4 Ga [38,46]. Textural studies have documented rare patches of feldspar in ALH-84001 that retain the outline of a feldspar crystal [17,47], have relic twins or cleavage [17], and/or are crystalline [47]. The geochemical data could be reconciled with the evidence for a high temperature glass flow event if the meteorite cooled quickly following that event. Both the geochemical and textural data also permit a late shock event that heterogeneously affected the rock, leaving isolated regions unheated and undeformed. Shock heterogeneity [48,49], in concert with brecciation and associated rotation of carbonates,

would also help to explain why the carbonate minerals are locally (on a scale of several mm and less) magnetized in the same direction (Fig. 8c) but are as a whole (on a scale of cm or more) magnetized in multiple directions (compare Figs. 1b and 8c,e).

To resolve these issues, we have used data from ^{40}Ar/^{39}Ar dating of ALH84001 feldspathic glass to place an upper limit on the temperatures it and nearby carbonates have experienced during the last 4 Gyr. Several different laboratories have shown that the meteorite's ^{40}Ar/^{39}Ar chronometer was last reset sometime between 3.9 and 4.3 Ga [50,51]. Unfortunately, these dates are statistically indistinguishable from the Rb/Sr and Pb/Pb ages of the carbonates (3.90 ± 0.04 Ga and 4.04 ± 0.1 Ga, respectively) [12], and so do not by themselves specify whether the carbonates formed before or after the ^{40}Ar/^{39}Ar chronometer was reset. Using thermochronological modeling of several limiting thermal histories of the meteorite, we have demonstrated in a companion manuscript [1] that most of ALH84001 feldspathic glass has not been heated $\sim > 350$–500°C and shocked to peak pressures $\sim > 1$ GPa since the glass was last melted. This indicates that most of ALH84001, including carbonate associated with the glass, has not been above these temperatures since 3.9–4.1 Ga.

6. The age of the magnetization in ALH84001

Any magnetite and pyrrhotite in carbonates heated during the last glass-melting event should therefore retain thermoremanent magnetizations that originated during that event. The magnetization of such carbonates must then have been acquired at 3.9–4.1 Ga (using the youngest possible ^{40}Ar/^{39}Ar date [51] as a lower limit on the age of the magnetization and the oldest date on the carbonates [12] as an upper limit). Because the shock at 4 Ga produced very high and long-lived post-shock temperatures (see above and [1]), any phase transitions that occurred during the shock itself are unlikely to have left metastable or otherwise nonthermal remanent magnetization (e.g., [9,52]) in the carbonates.

Any carbonates not heated during the last glass-melting event would retain nearly all of their magnetization acquired at the time of their formation at ~ 3.9–4.1 Ga. The latter carbonates could have a depositional, crystallization, or thermoremanent magnetization. That pyrrhotite and magnetite in ALH84001 carbonate have probably not been shocked $\sim > 1$ GPa since 4 Ga [1] demonstrates that they have not since been subject to shock-induced magnetization changes and phase transitions (occurring at pressures of > 1 GPa and > 1.6 GPa for magnetite and pyrrhotite, respectively [9,52]) which might otherwise alter their primary 4 Ga remanence. In summary, our results permit some carbonates to have been affected by localized heating since their formation. However, in most cases any such localized heating must have occurred very soon after their formation.

Our data show that most of the carbonates in ALH84001 should retain magnetizations they acquired at 3.9–4.1 Ga on Mars. Depending on their Curie points and rock magnetic properties, chromites located near feldspathic glass could retain a magnetization at least this old. Because chromites are believed to be primary igneous minerals in ALH84001, some of their magnetization could in fact be as old as the meteorite's crystallization age, 4.5 Gyr. On the other hand, the magnetization in the chromites may not have been acquired in a magnetic field (if the magnetization is simply the result of zero-field alignment along an easy axis) or else it could have been acquired in a field more recently (if the chromites have low Curie points and/or easily acquire viscous remanence). The fact that chromites are magnetized in different directions is consistent with zero-field remanence, but also with a scenario in which the chromites have experienced a range of thermal histories and/or have been rotated during one or more brecciation event since their formation. In the latter scenario, various grains may have reached temperatures exceeding their magnetic blocking temperatures at different times between 4.5 and 4.0 Ga, during which the relative orientation of the local magnetic field changed.

Such a heterogeneous thermal and deformational history is supported by textural observations that chromites within cataclastic granular bands of orthopyroxene (which contain many carbonates and so must predate 4 Ga) have been severely deformed into elongate anhedral stringers (e.g., chromite adjacent to carbonates at bottom of Fig. 8d), while chromites located outside these granular bands are rarely subhedral and less fractured (Fig. 8b,f). Additional evidence that some chromite may have escaped late heating comes from the identification of two regions in ALH-84001 with ^{40}Ar/^{39}Ar laser probe ages of 4.4 Ga [50]. Determining the exact age and origin of the magnetization in the chromites will require a detailed analysis of their magnetic properties combined with low blocking temperature geochronometers capable of placing thermal constraints directly on individual chromite grains.

7. Implications for the timing of the Martian dynamo

The magnetization in ALH84001 carbonates is the oldest ever identified in any planetary rock and the only well-dated remanence in a Martian sample. It is at least 400 Myr older than the oldest magnetization identified in an Earth rock [53]. We have shown (Section 3) that a typical ALH84001 zoned carbonate is composed of ~ 1 wt% pyrrhotite and magnetite in a mass ratio of ~ 0.3–0.5, and these are SD ($\sim 70\%$) and SP ($\sim 30\%$) in size [20]. Thus, the carbonates in ALH84001 should have a saturation IRM of $\sim 10^3$ A/m. Since our magnetization inversion demonstrates that the carbonates have NRMs of a few A/m (e.g., Fig. 9) we estimate that the ratio of their NRM to their IRM is ~ 0.1–1%. This estimate roughly agrees with the NRM to IRM ratios of $\sim 3\%$ directly measured for each of three bulk grains taken from the interior of ALH84001 [14] (the magnetization of such grains is likely to be dominated by any interior carbonates). A thermoremanent magnetization acquired by single domain magnetite grains in a field of 50 μT will generally be a few percent of IRM, while detrital remanence produced in the same field will be $\sim 0.1\%$ of IRM [54,55]. Thus, the NRM to IRM ratios of ALH84001 samples are consistent with an origin as a thermoremanent (detrital remanent) magnet-

ism in a field roughly 0.1–1 times (1–10 times) that at the surface of the present-day Earth. These values may be lower limits given the heterogeneous orientation of the magnetization in the meteorite (Figs. 7 and 8), and should be reproduced with more robust paleointensity experiments like that of Thellier-Thellier [28]. This magnetizing field would be adequate for magnetotaxis by the bacteria whose magnetofossils have been reported in ALH84001 [20], and may have been capable of producing the intensity of the magnetic anomalies [2] on the Martian surface.

Such a field is unlikely to have been that of the Sun, the solar wind, or other planets, whose total intensity is not thought to have been much larger than the present value (several nT) at Mars' current orbit 4 Ga [27]. Fields generated or amplified by impact-produced plasma [56,57] have never been conclusively demonstrated to occur in nature [58]. A simpler explanation is that ALH84001 was magnetized by either a Martian geodynamo or by local crustal remanent fields like those in the Martian southern hemisphere [2]. Since a Martian geodynamo field presumably produced the crustal magnetizations, our data imply that Mars had a magnetic field generated by an active geodynamo by at least 4 Ga. It is not clear if the dynamo still remained active at 4 Ga. This agrees with but is much more precise than the crater count ages (3.0–4.5 Ga, and most probably > 3.7 Ga) [59] inferred for the surfaces associated with the Martian crustal magnetizations. Our data do not support recent suggestions [3] that the Martian dynamo originated substantially after the formation of the large impact basins. Instead, our results are consistent with thermal evolution models of Mars that predict a convecting core and geodynamo extending from 4.55 Ga (or possibly delayed by several hundred Myr) to sometime after 4 Ga [60–64]. Because we are unable to determine whether the Martian dynamo was still active at 4 Ga, our results do not directly constrain the age of Hellas or other unmagnetized impact basins situated within the crustal magnetic anomalies. Given that chromites in the meteorite could retain a magnetic remanence that predates that of the carbonates, ALH84001 may contain records of Mar-

tian fields older than 4 Ga, possibly even dating back to near the time of planetary formation.

8. Summary

In the present manuscript we have demonstrated the following:

1. Magnetite and pyrrhotite within carbonates carry much of the magnetization in the interior of ALH84001.
2. The carbonates were magnetized prior to ~ 3.9 Ga.
3. The intensity of their magnetization gives evidence that a Martian dynamo was active at or prior to ~ 3.9 Ga.
4. The magnetization intensity implies a magnetic field on Mars of intensity within an order of magnitude of that at the surface of the present-day Earth.
5. Chromite in ALH84001 also retains a magnetization of unknown origin, stability, and age.

Acknowledgements

References

[1] B.P. Weiss, D.L. Shuster, S.T. Stewart, Temperatures on Mars from $^{40}Ar/^{39}Ar$ thermochronology of ALH84001, Earth Planet. Sci. Lett. 200 (2002) S0012-821x(02)00729-x.
[2] M. Acuna, J. Connerney, N. Ness, R. Lin, D. Mitchell, C.

Carlson, J. McFadden, K. Anderson, H. Reme, C. Mazelle, D. Vignes, P. Wasilewski, P. Cloutier, Global distribution of crustal magnetization discovered by the Mars Global Surveyor MAG/ER experiment, Science 284 (1999) 790–793.

[3] G. Schubert, C.T. Russell, W.B. Moore, Timing of the Martian dynamo, Nature 408 (2000) 666–667.

[4] D.W. Collinson, Magnetic properties of Martian meteorites – Implications for an ancient Martian magnetic field, Meteorit. Planet. Sci. 32 (1997) 803–811.

[5] D.W. Collinson, Magnetic properties of Antarctic shergottite meteorites EETA79001 and ALHA77005: Possible relevance to a Martian magnetic field, Earth Planet. Sci. Lett. 7 (1986) 159–164.

[6] S.M. Cisowski, Magnetism of meteorites, in: J.A. Jacobs (Ed.), Geomagnetism, vol. 2, Academic Press, London, 1987, pp. 525–560.

[7] S.M. Cisowski, Magnetic studies on Shergotty and other SNC meteorites, Geochim. Cosmochim. Acta 50 (1986) 1043–1048.

[8] T. Nagata, Paleomagnetism of Antarctic achondrites, Mem. Natl. Inst. Polar Res. Spec. Issue 17 (1980) 233–242.

[9] P. Rochette, J.P. Lorand, G. Fillion, V. Sautter, Pyrrhotite and the remanent magnetization of SNC meteorites: a changing perspective on Martian magnetism, Earth Planet. Sci. Lett. 190 (2001) 1–12.

[10] J. Shaw, M.J. Hill, S.J. Openshaw, Investigating the ancient Martian magnetic field using microwaves, Earth Planet. Sci. Lett. 190 (2001) 103–109.

[11] L.E. Nyquist, B. Bansal, H. Wiesmann, C.-Y. Shih, 'Martians' young and old: Zagami and ALH84001, Lunar Planet. Sci. XXVI (1995) 1065–1066.

[12] L.E. Borg, J.N. Connelly, L.E. Nyquist, C.Y. Shih, H. Wiesmann, Y. Reese, The age of the carbonates in martian meteorite ALH84001, Science 286 (1999) 90–94.

[13] M. Wadhwa, S.R. Sutton, G.J. Flynn, M. Newville, Microdistributions of Rb and Sr in ALH84001 carbonates: Chronological implications for secondary alteration on Mars, Lunar Planet. Sci. XXXIII (2002) abstract 1362.

[14] J.L. Kirschvink, A.T. Maine, H. Vali, Paleomagnetic evidence of a low-temperature origin of carbonate in the Martian meteorite ALH84001, Science 275 (1997) 1629–1633.

[15] B.P. Weiss, J.L. Kirschvink, F.J. Baudenbacher, H. Vali, N.T. Peters, F.A. MacDonald, J.P. Wikswo, A low temperature transfer of ALH84001 from Mars to Earth, Science 290 (2000) 791–795.

[16] B.P. Weiss, H. Vali, S.T. Stewart, J.L. Kirschvink, Records of an ancient Martian magnetic field in ALH84001, Lunar Planet. Sci. XXXII (2001) abstract 1244.

[17] A.H. Treiman, The history of Allan Hills 84001 revised: Multiple shock events, Meteorit. Planet. Sci. 33 (1998) 753–764.

[18] C.K. Shearer, L.A. Leshin, C.T. Adcock, Olivine in Martian meteorite Allan Hills 84001: Evidence for a high-temperature origin and implications for signs of life, Meteorit. Planet. Sci. 34 (1999) 331–339.

[19] J.P. Greenwood, H.Y. McSween, Petrogenesis of Allan Hills 84001: Constraints from impact-melted feldspathic and silica glasses, Meteorit. Planet. Sci. 36 (2001) 43–61.

[20] K.L. Thomas-Keprta, D.A. Bazylinski, J.L. Kirschvink, S.J. Clemett, D.S. McKay, S.J. Wentworth, H. Vali, E.K. Gibson Jr., C.S. Romanek, Elongated prismatic magnetite crystals in ALH84001 carbonate globules: Potential Martian magnetofossils, Geochim. Cosmochim. Acta 64 (2000) 4049–4081.

[21] B.P. Weiss, F.J. Baudenbacher, J.P. Wikswo, J.L. Kirschvink, Magnetic microscopy promises a leap in sensitivity and resolution, EOS Trans. AGU 82 (2001) 513 and 518.

[22] F.J. Baudenbacher, N.T. Peters, J.P. Wikswo, High resolution low-temperature superconductivity superconducting quantum interference device microscope for imaging magnetic fields of samples at room temperatures, Rev. Sci. Instrum. 73 (2002) 1247–1254.

[23] I.M. Thomas, T.C. Moyer, J.P. Wikswo, High resolution magnetic susceptibility imaging of geological thin sections: pilot study of a pyroclastic sample from the Bishop Tuff, Geophys. Res. Lett. 19 (1992) 2139–2142.

[24] R. Egli, F. Heller, High-resolution imaging using a high-Tc superconducting quantum interference device (SQUID) magnetometer, J. Geophys. Res. 105 (2000) 25709–25727.

[25] N.R. Nowaczyk, H.-U. Worm, A. Knecht, J.H. Hinken, Imaging distribution patterns of magnetic minerals by a novel high-Tc-SQUID-based field distribution measuring system: Applications to Permian sediments, Geophys. J. Int. 132 (1998) 721–726.

[26] H. Sakai, K. Shirai, M. Takani, M. Horii, M. Funaki, Analysis of fine structure of chert and BIF by measurement of high resolution magnetic field and scanning x-ray analyzed microscope, Proc. NIPR Symp. Antarc. Geosci. 10 (1997) 59–67.

[27] D.J. Dunlop, O. Ozdemir, Rock Magnetism: Fundamentals and Frontiers, Cambridge University Press, New York, 1997, 573 pp.

[28] R.S. Coe, S. Grommé, E.A. Mankinen, Geomagnetic paleointensities from radiocarbon-dated lava flows on Hawaii and the question of the Pacific nondipole low, J. Geophys. Res. 83 (1978) 1740–1756.

[29] R.S. Coe, The effect of magnetic interactions on paleointensity determination by the Thellier's method, J. Geomag. Geoelectr. 26 (1974) 311–317.

[30] J.M. Eiler, J.W. Valley, C.M. Graham, J. Fournelle, Two populations of carbonate in ALH84001: Geochemical evidence for discrimination and genesis, Geochim. Cosmochim. Acta 66 (2002) 1285–1303.

[31] R.A. Langel, W.J. Hinze, The Magnetic Field of the Earth's Lithosphere, Cambridge University Press, Cambridge, 1998, 429 pp.

[32] M.E. Purucker, T.J. Sabaka, R.A. Langel, Conjugate gradient analysis: a new tool for studying satellite magnetic data sets, Geophys. Res. Lett. 23 (1996) 507–510.

[33] W.H. Press, S.A. Teukolsky, W.T. Vetterling, B.P. Flannery, Numerical Recipes in Fortran 77: The Art of Scientific Computing, Cambridge University Press, Cambridge, 1992, 933 pp.

[34] D.W. Mittlefehldt, ALH84001, a cumulate orthopyroxenite member of the Martian meteorite clan, Meteoritics 29 (1994) 214–221.

[35] A. Kumar, M.S. Bhalla, A source of stable remanence in chromite ores, Geophys. Res. Lett. 11 (1984) 177–180.

[36] Y.J. Yu, D.J. Dunlop, O. Ozdemir, H. Ueno, Magnetic properties of Kurokami pumices from Mt. Sakurajima, Japan, Earth Planet. Sci. Lett. 192 (2001) 439–446.

[37] A.H. Treiman, Heterogeneity of remanent magnetism in ALH84001: petrologic constraints, Lunar Planet. Sci. XXXI (2000) abstract 1225.

[38] J.W. Valley, J.M. Eiler, C.M. Graham, E.K. Gibson, C.S. Romanek, E.M. Stolper, Low-temperature carbonate concretions in the Martian meteorite ALH84001: Evidence from stable isotopes and mineralogy, Science 275 (1997) 1633–1638.

[39] H.Y. McSween, R.P. Harvey, An evaporation model for formation of carbonates in the ALH84001 Martian meteorite, Int. Geol. Rev. 40 (1998) 774–783.

[40] E.R.D. Scott, A.N. Krot, A. Yamaguchi, Carbonates in fractures of Martian meteorite Allan Hills 84001: Petrologic evidence for impact origin, Meteorit. Planet. Sci. 33 (1998) 709–719.

[41] J.P. Bradley, H.Y. McSween, R.P. Harvey, Epitaxial growth of nanophase magnetite in Martian meteorite, Meteorit. Planet. Sci. 33 (1998) 765–773.

[42] A. Schult, Effect of pressure on the Curie temperature of titanomagnetites $[(1-x)Fe_3O_4-xTiFe_2O_4]$, Earth Planet. Sci. Lett. 10 (1970) 81–86.

[43] T. Cooney, E. Scott, A. Krot, S. Sharma, A. Yamaguchi, Vibrational spectroscopic study of minerals in the Martian meteorite ALH84001, Am. Mineral. 84 (1999) 1569–1576.

[44] A. Bischoff, D. Stoffler, Shock metamorphism as a fundamental process in the evolution of planetary bodies: Information from meteorites, Eur. J. Mineral. 4 (1992) 707–755.

[45] T. Sekine, T.S. Duffy, A.M. Rubin, W.W. Anderson, T.J. Ahrens, Shock compression and isentropic release of granite, Geophys. J. Int. 120 (1995) 247–261.

[46] A.J.R. Kent, I.D. Hutcheon, F.J. Ryerson, D.L. Phinney, The temperature of formation of carbonate in Martian meteorite ALH84001: Constraints from cation diffusion, Geochim. Cosmochim. Acta 65 (2001) 311–321.

[47] D.A. Kring, T.D. Swindle, J.D. Gleason, J.A. Grier, Formation and relative ages of maskelynite and carbonate in ALH84001, Geochim. Cosmochim. Acta 62 (1998) 2155–2166.

[48] M.R. Baer, Computational modeling of heterogeneous reactive materials at the mesoscale, in: M.D. Furnish, L.C. Chhabildas, R.S. Hixson (Eds.), Eleventh Conference on Shock Compression of Condensed Matter, American Institute of Physics, Snowbird, UT, 1999, pp. 27–33.

[49] V. Malavergne, F. Guyot, K. Benzerara, I. Martinez, Description of new shock-induced phases in the Shergotty, Zagami, Nakhla and Chassigny meteorites, Meteorit. Planet. Sci. 36 (2001) 1297–1305.

[50] G. Turner, S.F. Knott, R.D. Ash, J.D. Gilmour, Ar-Ar chronology of the Martian meteorite ALH84001: Evidence for the timing of the early bombardment of Mars, Geochim. Cosmochim. Acta 61 (1997) 3835–3850.

[51] D.D. Bogard, D.H. Garrison, Argon-39-argon-40 'ages' and trapped argon in Martian shergottites, Chassigny, and Allan Hills 84001, Meteorit. Planet. Sci. 34 (1999) 451–473.

[52] S.A. Gilder, M. LeGoff, J. Peyronneau, J.-C. Chervin, Novel high pressure magnetic measurements with application to magnetite, Geophys. Res. Lett. 29 (2002) 10.1029/2001GL014227.

[53] C.J. Hale, D.J. Dunlop, Evidence for an early Archean geomagnetic field: A paleomagnetic study of the Komati Formation, Barberton greenstone belt, South Africa, Geophys. Res. Lett. 11 (1984) 97–100.

[54] M. Hart, M. Fuller, Magnetization of a dolomite bed in the Monterey Formation: Implications for diagenesis, Geophys. Res. Lett. 15 (1988) 491–494.

[55] M. Fuller, S. Cisowski, M. Hart, R. Haston, E. Schmidke, R. Jarrard, NRM:IRM(s) demagnetization plots; an aid to the interpretation of natural remanent magnetization, Geophys. Res. Lett. 15 (1988) 518–521.

[56] D.A. Crawford, P.H. Schultz, Laboratory observations of impact-generated magnetic fields, Nature 336 (1988) 50–52.

[57] L.L. Hood, Z. Huang, Formation of magnetic-anomalies antipodal to lunar impact basins – 2-Dimensional model-calculations, J. Geophys. Res. 96 (1991) 9837–9846.

[58] D.W. Collinson, Magnetism of the Moon – a lunar core dynamo or impact magnetization?, Surv. Geophys. 14 (1993) 89–118.

[59] W.K. Hartmann, G. Neukum, Cratering chronology and the evolution of Mars, Space Sci. Rev. (2001) 165–194.

[60] D.J. Stevenson, T. Spohn, G. Schubert, Magnetism and thermal evolution of the terrestrial planets, Icarus 54 (1983) 466–489.

[61] G. Schubert, T. Spohn, Thermal history of Mars and the sulfur content of its core, J. Geophys. Res. 95 (1990) 14095–14104.

[62] F. Nimmo, D. Stevenson, Influence of early plate tectonics on the thermal evolution and magnetic field of Mars, J. Geophys. Res. 105 (2000) 11969–11979.

[63] D.J. Stevenson, Mars core and magnetism, Nature 412 (2001) 214–219.

[64] M.T. Zuber, The crust and mantle of Mars, Nature 412 (2001) 220–227.

[65] R.F. Butler, S.K. Banerjee, Theoretical single-domain size range in magnetite and titanomagnetite, J. Geophys. Res. 80 (1975) 4049–4058.

[66] J.C. Diaz Ricci, J.L. Kirschvink, Magnetic domain state and coercivity predictions for biogenic greigite (Fe_3S_4): A comparison of theory with magnetosome observations, J. Geophys. Res. 97 (1992) 17309–17315.